CrystEngComm

COMMUNICATION

View Article Online
View Journal | View Issue

Cite this: *CrystEngComm*, 2015, **17**, 6269

Received 18th May 2015,
Accepted 13th July 2015

DOI: 10.1039/c5ce00956a

www.rsc.org/crystengcomm

Hetero-epitaxial growth of stoichiometry tunable $Si_{1-x}Ge_x$ film *via* a low temperature aluminium-induced solid phase epitaxy (Al-SPE) process†

Chuan-Jung Lin,[a] Sung-Yen Wei,[b] Chien-Chung Hsu,[a] Sheng-Min Yu,[ab] Wen-Ching Sun,[b] Tzer-Shen Lin[b] and Fu-Rong Chen*[a]

A novel process of aluminum-induced solid-phase epitaxy (Al-SPE) is used to fabricate a hetero-epitaxial $Si_{1-x}Ge_x$ (epi-SiGe) film on an sc-Si (100) substrate at relatively low temperatures (lower than 450 °C) using a 1/4 × 4″ wafer. The stoichiometry of Ge in the epi-SiGe film can be easily tuned in the Al-SPE process by controlling the annealing temperature and the Ge fraction (x) of the initial a-$Si_{1-x}Ge_x$ layer. The stoichiometry and epitaxial relationship of the epi-SiGe film were verified by grazing incidence X-ray diffraction (GI-XRD) and transmission electron microscopy (TEM). The Al-SPE mechanism is directly verified by *in situ* heating TEM. Based on the experimental results, it is concluded that the Al-SPE mechanism for the epi-SiGe film can be divided into four steps: (a) initial stage; (b) formation of a-$Si_{1-x}Ge_x$ free atoms and diffusion along Al grain boundaries to the sc-(100) substrate surface; (c) nucleation of crystalline $Si_{1-x}Ge_x$ at the surface of the sc-Si (100) substrate; and (d) crystal growth and layer exchange.

Recently, the hetero-epitaxial growth of silicon–germanium (epi-SiGe) thin films directly on silicon (Si) substrate has received a great deal of attention due to the fact that its energy band gap and lattice constant can be linearly tuned with germanium (Ge) fractions. Epi-SiGe films on Si substrate can have unique applications in many different fields, for example, as virtual substrates for MOSFETs to increase carrier mobility,[1] buffer layers for reducing defect density,[2] or templates for type III–V high-efficiency solar cells.[3] However, the epi-SiGe film on Si substrate is usually prepared by chemical vapor deposition (CVD)[4] or molecular beam epitaxy (MBE)[5] utilizing an ultra-high vacuum system and involving high temperature reaction with toxic precursors, such as silane (SiH_4), germane (GeH_4), *etc.* Although solid state ion implantation in general offers a non-toxic process, it still requires a follow-up process at high temperature and high vacuum (900–1000 °C) for recrystallization.[6] In the past decades, aluminium-induced crystallization (AIC), a low-cost and non-toxic process, has been shown to be a potential method to fabricate large grain sized (~10 to 100 μm), orientation-controlled, and self-organized poly-Si, poly-$Si_{1-x}Ge_x$, and poly-Ge films on foreign (non-sc-Si) substrates at temperatures lower than the eutectic temperature (Al–Si: 577 °C; Al–Ge: 420 °C).[7–12] When the sc-Si (100) substrate is used, the process temperature can be significantly further reduced (depending on the Ge fraction) for epi-SiGe films.[13] The Al-SPE of the $Si_{1-x}Ge_x$ epitaxial layer with a stacking structure of the a-Ge/Al/sc-Si (100) substrate has been demonstrated by Z. Liu *et al.*[13,14] However, the molar fraction of Ge in the epi-SiGe film cannot be accurately controlled due to the fact that the contribution of Si to the epi-SiGe film comes from the sc-Si (100) substrate. Therefore, the growth of gradient lattice match epi-SiGe films for reducing dislocation density cannot be achieved. In this paper, the stoichiometry of the epi-SiGe film obtained *via* Al-SPE is controlled using the a-$Si_{1-x}Ge_x$ layer as the starting layer rather than a pure Ge layer as reported previously.[13–15] An AlO_x layer between a-$Si_{1-x}Ge_x$ and Al layers is intentionally employed as a diffusion barrier to control the reaction rate in order to achieve an optimum epitaxial SiGe film. Here we show that the molar fraction of Ge in the epi-SiGe film depends on the initial Ge fraction (x) in the a-$Si_{1-x}Ge_x$ layer and the annealing temperature of the Al-SPE process. The success of this process offers a possibility to prepare epi-SiGe buffer layers with gradient lattice constant to avoid lattice mismatch in the future.

In this study, a p-type sc-Si (100) wafer (size of 1/4 × 4″ wafer) is used as the substrate. It is cleaned with a chemical solution containing RCA I, RCA II, and Piranha.[16] After chemical cleaning, the wafer is dipped into 5% HF for 5 minutes at room temperature to remove native oxide and dried with nitrogen gas (N_2). In order to verify the effect of the initial

[a] *Department of Engineering and System Science, National Tsing Hua University, Hsinchu 30013, Taiwan, ROC. E-mail: frchen@ess.nthu.edu.tw; Fax: (+886) 3 5734066; Tel: (+886) 3 5715131 Ext. 62247*
[b] *Material and Chemical Research Laboratories, Industrial Technology Research Institute, Chutung, Hsinchu 31040, Taiwan, ROC*

† Electronic supplementary information (ESI) available: EDX results of SiGe-50 and SiGe-75 before annealing; Raman shift results; SIMS results of SiGe-50 and SiGe-75 before and after annealing. See DOI: 10.1039/c5ce00956a

stoichiometry of Ge on the final epi-SiGe film, samples with stacking structures of a-$Si_{1-x}Ge_x$ (300 nm)/Al (300 nm)/sc-Si (100) (x = 0.5 and 0.75) are prepared from an Al target (5N) and a SiGe alloy target (4N) at room temperature by DC- and RF-sputtering, respectively. These samples are labelled as "SiGe-50" and "SiGe-75", respectively. Moreover, the Ge fraction of the initial a-$Si_{1-x}Ge_x$ layer is measured by EDX (Fig. S1(a) and (b)†). The base and sputtering pressures are respectively set at 2×10^{-6} and 3×10^{-3} torr. An AlO_x layer is intentionally formed on top of the Al layer by exposing the Al layer to air for 2 minutes before the a-$Si_{1-x}Ge_x$ layer is deposited onto the Al layer.[17] After deposition of the a-$Si_{1-x}Ge_x$ layer, these samples are annealed at 450 °C in a tube furnace for 10 hours under argon (Ar) atmosphere. Schematic diagrams of the AI-SPE process for these stacking structures are shown in Fig. 1(a). Fig. 1(a)(top) shows the initial stacking structure before the AI-SPE process. Fig. 1(a) (bottom) shows that after the AIC process, the layer exchange between the Al layer and a-$Si_{1-x}Ge_x$ is completed. The epi-SiGe film on sc-Si (100) and an upper layer containing the mixture of exchanged Al grains and residual a-$Si_{1-x}Ge_x$ are formed. In this paper, we have utilized analytical tools such as electron backscatter diffraction (EBSD; Oxford Instruments), secondary ion mass spectrometry (SIMS; ION-TOF), Raman spectroscopy (LABRAM HR 800 UV), transmission electron microscopy (TEM; JEOL-2010F) and grazing incidence X-ray diffraction (GI-XRD; Bede D1) to extract detail information about the crystal structure, crystallographic relationship and stoichiometry of Ge within the epi-SiGe film. Before EBSD analysis, the mixture layer is removed using an Al etching solution containing H_3PO_4, HNO_3, CH_3COOH, and H_2O (3 : 3 : 1 : 1).[18,19]

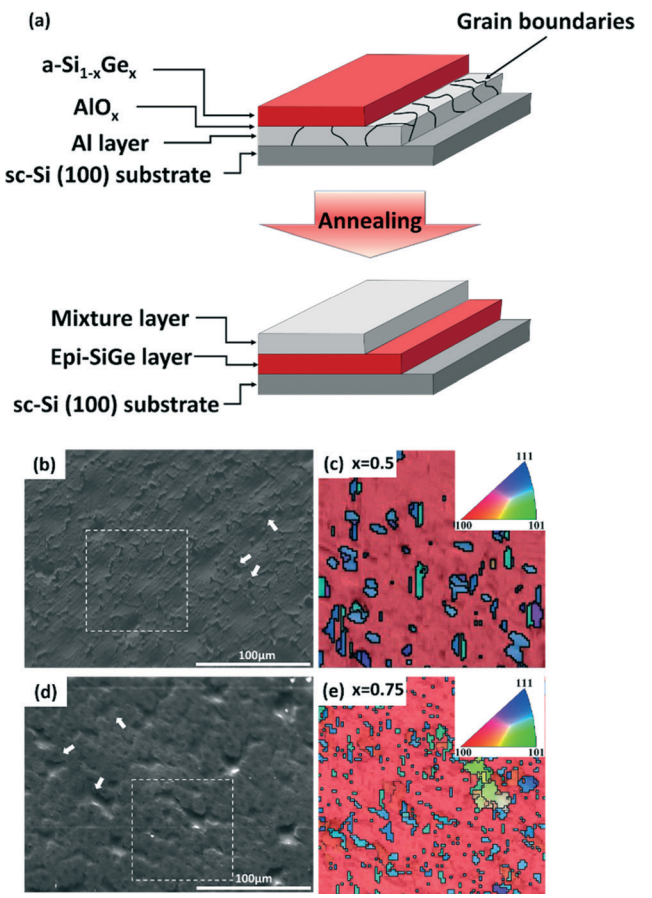

Fig. 1 (a) Schematic diagrams of the AI-SPE process for the hetero-epitaxial growth of the epi-SiGe film on the Si (100) substrate; (b) and (c) are the scanning electron microscopy (SEM) image and crystallographic orientation map of SiGe-50 after removal of the mixture layer, respectively; (d) and (e) are the SEM image and crystallographic orientation map of SiGe-75 after removal of the mixture layer, respectively. The insets in (c) and (e) are the colour indices of the crystallographic orientation.

The two factors that affect the Ge stoichiometry of the epi-SiGe film can be controlled by the initial composition of Ge in the a-$Si_{1-x}Ge_x$ film and the treatment temperature of the AI-SPE process. This is discussed as follows.

(a) Controlling the stoichiometry of Ge : Ge composition of the initial amorphous layer

Fig. 1(c) and (e) show the EBSD crystallographic orientation maps of SiGe-50 and SiGe-75 samples after removal of the mixture layer, respectively. The insets in Fig. 1(c) and (e) are the colour indices for the preferred crystallographic orientation. Based on the colour index, approximately 95% of the entire area (50 × 50 μm^2) is in the (100) orientation, indicating that both SiGe-50 and SiGe-75 have continuous epi-SiGe films grown on the sc-Si (100) substrate. However, a small population of [111] and [110] orientations (blue and green patches) is also observed in Fig. 1(c) and (e), which may be attributed to the secondary island (labeled with white arrows in Fig. 1(b) and (d)) induced after the removal of the mixture layer.

The Raman spectra with an excitation wavelength of 514 nm are used to evaluate the fine structure of the epi-SiGe film for SiGe-50 and SiGe-75 samples at room temperature, as shown in Fig. S2.† The Raman peaks for SiGe-50 are clearly located at approximately 288, 399, and 474 cm^{-1}, while the Raman peaks for SiGe-75 are clearly visible at 295, 406, and 482 cm^{-1}. These peaks correspond to the signal of Ge–Ge, Si–Ge, and Si–Si bond modes, respectively.[13] It is worth noting that the Si–Ge peak shifts from 399 cm^{-1} (SiGe-50) to 406 cm^{-1} (SiGe-75), indicating that a higher Ge fraction exists in SiGe-75.[20] Fig. S3(a) to (d),† the SIMS depth profiles for samples of SiGe-50 and SiGe-75 before and after annealing, show that a layer exchange takes place between the a-$Si_{1-x}Ge_x$ and Al layers of both samples. The signals of a-$Si_{1-x}Ge_x$ and Al are effectively sharp across the interface before the layer exchange (Fig. S3(a) and (c)†) in the AI-SPE process. After the AI-SPE process was completed, the a-$Si_{1-x}Ge_x$ layer exchanged with the Al layer (Fig. S3(b) and (d)†). In addition, the SIMS profiles in Fig. S3(b) and (d)† can be divided into three regions: (i) mixture layer; (ii) epi-SiGe film; and (iii) sc-Si (100) substrate. As shown, Ge has a peak-shaped distribution

in the epi-SiGe film after the layer exchange. Moreover, it is interesting to note that the Al atoms are uniformly distributed in the epi-SiGe film, in which case Al plays the role of a p-type dopant in the epi-SiGe film after the AI-SPE process. In this case, the fraction of Al in the epi-SiGe film (approximately 3×10^{18} cm^{-3} at temperatures below 450 °C) is high enough to allow the epi-SiGe film to be used as a back surface field (BSF) for solar cell application, and it has been verified in our earlier study.[18,19]

The direct evidence of the layer exchange between the initial a-$Si_{1-x}Ge_x$ layer with the Al layer and the epi-SiGe film epitaxially grown on the sc-Si (100) substrate can be seen from the TEM images. Fig. 2(a) and (b) show the TEM images of SiGe-50 before and after the AI-SPE process, respectively. In Fig. 2(a), the initial stacking structure of the a-$Si_{1-x}Ge_x$/Al/sc-Si (100) substrate can clearly be observed. The average thickness of the a-$Si_{1-x}Ge_x$ and Al layers is estimated to be around 300 nm. The inset in Fig. 2(a) shows the amorphous diffraction pattern recorded from the dashed circle in the a-$Si_{1-x}Ge_x$ layer. On the other hand, we can clearly see in Fig. 2(b) that the Al layer swaps its position with a-$Si_{1-x}Ge_x$ after the AI-SPE process and becomes a mixture layer (Al, a-$Si_{1-x}Ge_x$). Simultaneously, a-$Si_{1-x}Ge_x$ transforms into the epi-SiGe film on top of the sc-Si (100) substrate. The thickness of the epi-SiGe film for SiGe-50 is estimated to be around 300 nm which depends on the initial thickness of the a-$Si_{1-x}Ge_x$ and Al layers. The inset diffraction pattern in Fig. 2(b) is recorded from the region of the dashed circle. This diffraction pattern gives evidence that the epi-SiGe film indeed hetero-epitaxially grows on sc-Si (100). Fig. 2(c) shows the EDX map acquired from the area of the large dotted rectangular box in Fig. 2(b). In Fig. 2(c), Al, Ge, and Si are colour coded as blue, green, and red, respectively. From the EDX map, it is evident that Ge is uniformly distributed in the epi-SiGe film. The HRTEM image recorded from the region of the small dotted box in Fig. 2(d) reveals the epitaxial relationship of the epi-SiGe film with the sc-Si (100) substrate. From the HRTEM image (Fig. 2(d)) with internal reference of Si lattice spacing, the lattice constant of SiGe-50 is determined to be about 5.53 Å, corresponding to the Ge fraction within the epi-SiGe film which is approximately 0.49 (x = 0.49), as deduced from Vegard's law.[21] An AlO_x layer is observed at the interface between the epi-SiGe film and the sc-Si (100) substrate, and it will be illustrated in detail in a later paragraph.

The microstructure of SiGe-75 was analysed in the same way as SiGe-50. Fig. 3(a) and (b) are the cross-sectional TEM images of SiGe-75 before and after the AI-SPE process, respectively. The average thickness of the a-$Si_{1-x}Ge_x$ layer and Al layer is about 300 nm. The same as the case of SiGe-50, the atoms of the a-$Si_{1-x}Ge_x$ (x = 0.75) layer diffuse along the Al grain boundaries to the sc-Si (100) substrate,[22] and are converted to the crystalline epi-SiGe film (see inset diffraction pattern) after the AI-SPE process. The EDX map (Fig. 3(c)) acquired from the large dotted box also shows that Ge is uniformly spread in the epi-SiGe film. The HRTEM image

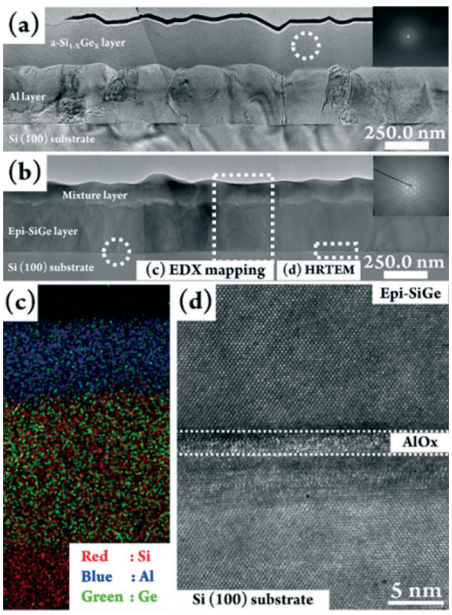

Fig. 2 (a) Cross-sectional TEM image of the SiGe-50 sample before the AI-SPE process; the magnification is set at 30k×; (b) cross-sectional TEM image of the SiGe-50 sample after the AI-SPE process. The insets in (a) and (b) are the selected area diffraction patterns (SADP) obtained from the dashed circle; (c) EDX map from the region of the large dotted box in (b); Al, Ge and Si are colour coded as blue, green, and red, respectively; (d) is the HRTEM image obtained from the small dotted rectangular box in (b).

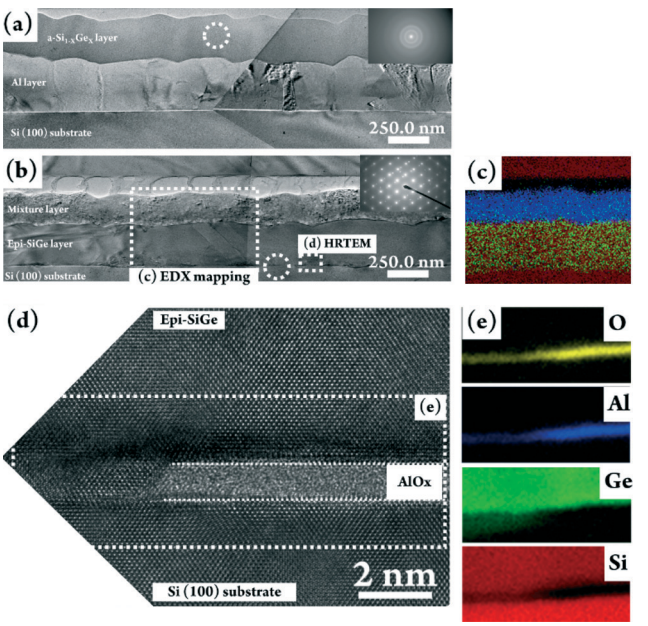

Fig. 3 (a) Cross-sectional TEM image of the SiGe-75 sample before annealing; magnification is at 30k×; (b) cross-sectional TEM image of the SiGe-75 sample after annealing; (c) EDX maps of the epi-SiGe film acquired from the large dotted box in (b); Al, Ge and Si are colour coded as blue, green, and red, respectively; (d) high-resolution TEM image recorded from the small dotted box in (b), showing the amorphous AlO_x interfacial layer present between epi-SiGe and substrate; (e) EELS maps of Al, Ge, Si, and O colour coded as blue, green, red, and yellow, respectively.

(Fig. 3(d)) recorded from the area of the small dotted rectangular box reveals the epitaxial relationship of the epi-SiGe film in the SiGe-75 sample even with the presence of an amorphous interfacial layer. The lattice constant of this epi-SiGe film is determined from the HRTEM image to be approximately 5.60 Å, corresponding to the Ge fraction within the epi-SiGe film which is approximately 0.72 (x = 0.72) according to Vegard's law.[21] The EELS maps in Fig. 3(e) confirmed that this interfacial layer is the AlO_x layer resulting from the exposure of Al to air (barrier control layer). The EELS maps of Al, Ge, Si, and O in Fig. 3(e) are colour coded as blue, green, red, and yellow, respectively.

(b) Controlling the stoichiometry of Ge: temperature effect

In order to understand the effect of temperature in the AI-SPE process on the final Ge fraction in the epi-SiGe film, the samples SiGe-50 and SiGe-75 were heat-treated at various temperatures from 25 °C to 450 °C. The variation of the lattice constant of epi-SiGe at different temperatures was analysed by grazing incidence X-ray diffraction (GID).

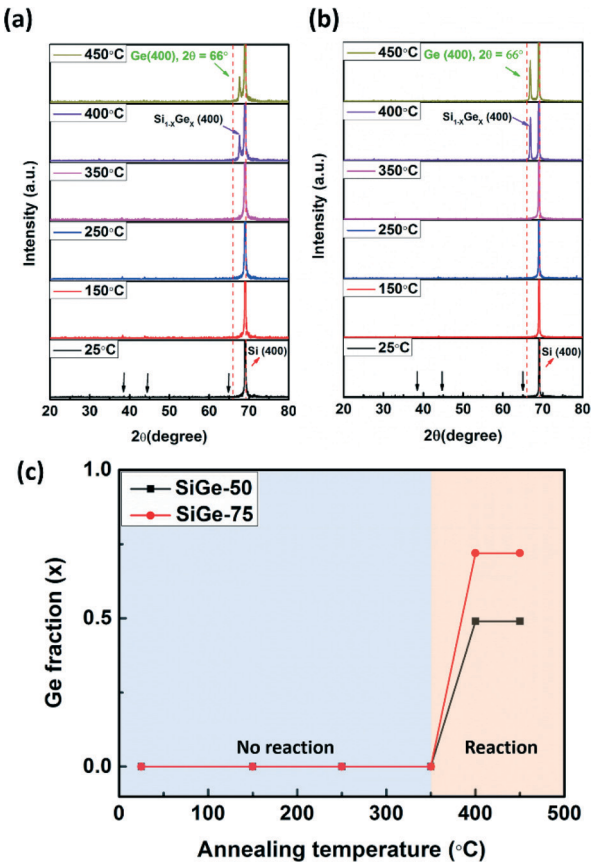

Fig. 4 Grazing incidence X-ray diffraction (GID) patterns of the as-deposited samples with Ge fractions (a) x = 0.5 and (b) x = 0.75 annealed at various temperatures from 25 °C to 450 °C; the figure inserts in (a) and (b) are recorded from the dashed rectangle; (c) is the plot of the Ge fraction (x) with respect to the annealing temperature from 25 °C to 450 °C, respectively.

Fig. 4(a) and (b) show the 2θ XRD patterns of SiGe-50 and SiGe-75 samples when *in situ* annealed at 25 °C, 150 °C, 250 °C, 350 °C, 400 °C, and 450 °C for 1h. For temperatures below 400 °C, the three very weak peaks located at 2θ 38.47°, 44.72°, and 65.02° corresponding to (111), (200), and (220) of Al diffractions are indicated with black arrows.[13] The strong diffraction peak which appeared at 69.2°, corresponding to Si (400), is indicated with a red arrow. As the annealing temperature exceeds 400 °C, an extra diffraction peak associated with $Si_{1-x}Ge_x$ (400) appears between Ge (400) (at 66°) and Si (400) (at 69.2°) for both SiGe-50 and SiGe-75 samples (this regain is marked by a red dashed line). Moreover, no other $Si_{1-x}Ge_x$ diffraction peaks can be observed in the XRD pattern which implies that the epi-SiGe film is hetero-epitaxially grown on the Si (100) substrate.[13] For the SiGe-50 sample, the initial Ge fraction is 0.5 (x = 0.5) and the diffraction peak of $Si_{1-x}Ge_x$ (400) annealed at 400 °C and 450 °C is almost located in the same position. This suggests that the lattice constant is maintained at 5.53 Å, corresponding to the Ge fraction which is approximately 0.49 (x = 0.49), as deduced from Vegard's law.[21] This result is in good agreement with the TEM data. Consistent with the results from the HRTEM analysis, the GID of SiGe-75 (Fig. 4(b)) shows that the lattice constant of the epi-SiGe film is approximately 5.60 Å, corresponding to the Ge fraction which is approximately 0.72 (x = 0.72), as deduced from Vegard's law,[21] when the annealing temperature is at 400 °C and 450 °C. Fig. 4(c) shows the plot of the Ge fraction with respect to the annealing temperature from 25 °C to 450 °C. From these results, it is evidently shown that the Ge fraction (lattice constant) within epi-SiGe can be easily controlled depending on the initial Ge fraction and annealing temperature.

In order to understand the mechanism of AI-SPE in detail, an *in situ* heating experiment is performed in a transmission electron microscope (*in situ* TEM). The results are summarized in Fig. 5(a) to (d). Before heating, the stacking layer of the a-$Si_{1-x}Ge_x$/Al/sc-Si (100) substrate can be clearly identified and are displayed in Fig. 5(a). As the temperature increases to 450 °C (5 °C min^{-1}), the Al grain boundaries disappear which may suggest that a-$Si_{1-x}Ge_x$ decomposes into the form of free atoms that diffuse along Al grain boundaries into the Al layer (Fig. 5(b)). As the free atoms continuously diffuse

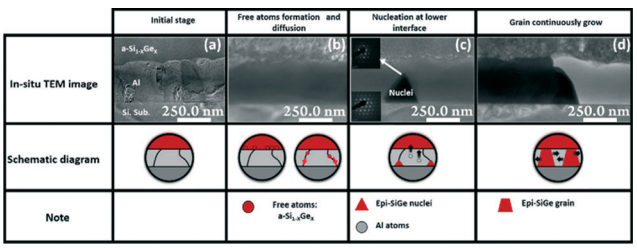

Fig. 5 *In situ* heating TEM observation of the AI-SPE mechanism. The mechanism can be divided into four steps: (a) initial stage; (b) free atom formation and diffusion along Al grain boundaries to the sc-(100) substrate surface; (c) nucleation at the surface of the sc-Si (100) substrate; (d) crystal growth and layer exchange.

across the Al layer and accumulate up to the saturation concentration of precipitation, nuclei form at the interface between Al and the sc-Si (100) substrate (Fig. 5(c)). This diffraction pattern inserted in Fig. 5(c) gives evidence that the nuclei indeed hetero-epitaxially grow on sc-Si (100). Furthermore, because the channel is formed, once the free atoms are continuously supplied from a-$Si_{1-x}Ge_x$ during the layer exchange (Al and a-$Si_{1-x}Ge_x$) process, the epi-SiGe nuclei start to grow until adjacent grains touch each other and form a continuous film (Fig. 5(d)). Finally, the layers of Al and epi-SiGe will change their positions.[13,14,23–27]

Conclusions

In this research, we demonstrated that a continuous SiGe film can be hetero-epitaxially grown on a large 1/4 × 4″ sc-Si (100) wafer at low-temperatures *via* an aluminium-induced solid-phase epitaxy process (Al-SPE). The stoichiometry of Ge in the epi-SiGe film can be controlled by the Ge composition in the initial a-$Si_{1-x}Ge_x$ layer and the process temperature. The epitaxial relationship of the epi-SiGe film is verified using EBSD, HRTEM, and GI-XRD techniques. Moreover, the mechanism of AI-SPE can be summarized in four steps which have been demonstrated by *in situ* heating TEM.

References

1 M. Junichi and O. Shoichi, *Jpn. J. Appl. Phys.*, 1994, **33**, 2290.
2 G. Wohl, V. Dudek, M. Graf, H. Kibbel, H. J. Herzog and M. Klose, *Thin Solid Films*, 2000, **369**, 175–181.
3 S. A. Ringel, J. Carlin, C. Andre, M. Hudait, M. Gonzalez, D. Wilt, E. Clark, P. Jenkins, D. Scheiman and A. Allerman, *Progr. Photovolt.: Res. Appl.*, 2002, **10**, 417–426.
4 B. M. H. Ning and J. E. Crowell, *Appl. Phys. Lett.*, 1992, **60**, 2914–2916.
5 J. Kuchenbecker, H. Kibbel, P. Muthsam and U. Konig, *Thin Solid Films*, 2001, **389**, 146–152.
6 W. J. Qi, B. Z. Li, G. B. Jiang, Z. G. Gu, T. K. Kwok, R. J. Zhang and P. K. Chu, *Thin Solid Films*, 1997, **293**, 310–314.
7 K. Toko, N. Fukata, K. Nakazawa, M. Kurosawa, N. Usami, M. Miyao and T. Suemasu, *J. Cryst. Growth*, 2013, **372**, 189–192.
8 K. Toko, K. Nakazawa, N. Saitoh, N. Yoshizawa, N. Usami and T. Suemasu, *Cryst. Growth Des.*, 2013, **13**, 3908–3912.
9 R. Numata, K. Toko, N. Saitoh, N. Yoshizawa, N. Usami and T. Suemasu, *Cryst. Growth Des.*, 2013, **13**, 1767–1770.
10 K. Toko, K. Nakazawa, N. Saitoh, N. Yoshizawa, N. Usami and T. Suemasu, *CrystEngComm*, 2014, **16**, 2578–2583.
11 K. Toko, K. Nakazawa, N. Saitoh, N. Yoshizawa and T. Suemasu, *CrystEngComm*, 2014, **16**, 9590–9595.
12 M. Kurosawa, N. Kawabata, T. Sadoh and M. Miyao, *ECS J. Solid State Sci. Technol.*, 2012, **1**, P144–P147.
13 Z. Liu, X. Hao, F. Qi, A. Ho-Baillie and M. A. Green, *Scr. Mater.*, 2014, **71**, 25–28.
14 Z. Liu, X. Hao, A. Ho-Baillie and M. A. Green, *Appl. Phys. Lett.*, 2014, **104**(5), DOI: 10.1063/1.4864463.
15 G. Ramanath, H. Z. Xiao, S. L. Lai, L. H. Allen and T. L. Alford, *J. Appl. Phys.*, 1996, **79**, 3094–3102.
16 H. Okumura, T. Akane, Y. Tsubo and S. Matsumoto, *J. Electrochem. Soc.*, 1997, **144**, 3765–3768.
17 T. Zhang, F. Ma and K. Xu, *Effect of Oxide Layer on Al-induced Crystallization of Amorphous Si(1-x)Ge(x) Thin Films*, 2010.
18 S.-Y. Wei, H.-H. Lin, S.-M. Yu, C.-K. Hsieh, S.-C. Tsai, W.-C. Sun, T.-S. Lin, C.-H. Tsai and F.-R. Chen, *CrystEngComm*, 2013, **15**, 1680–1684.
19 S.-Y. Wei, S.-M. Yu, L.-C. Yu, W.-C. Sun, C.-K. Hsieh, T.-S. Lin, C.-H. Tsai and F.-R. Chen, *CrystEngComm*, 2012, **14**, 4967–4971.
20 P. M. Mooney, F. H. Dacol, J. C. Tsang and J. O. Chu, *Appl. Phys. Lett.*, 1993, **62**, 2069–2071.
21 J. P. Dismukes, L. Ekstrom and R. J. Paff, *J. Phys. Chem.*, 1964, **68**, 3021–3027.
22 Z. M. Wang, J. Y. Wang, L. P. H. Jeurgens and E. J. Mittemeijer, *Surf. Interface Anal.*, 2008, **40**, 427–432.
23 C. A. Niedermeier, Z. Wang and E. J. Mittemeijer, *Acta Mater.*, 2014, **72**, 211–222.
24 A. Sakic, Y. Civale, L. K. Nanver, C. Biasotto and V. Jovanovic, *MRS Proceedings*, 2010, **1245**, DOI: 10.1557/PROC-1245-A20-03.
25 Y. Civale, G. Vastola, L. K. Nanver, R. Mary-Joy and J.-R. Kim, *J. Electron. Mater.*, 2009, **38**, 2052–2062.
26 Y. Civale, L. K. Nanver, P. Hadley, E. J. Goudena and H. Schellevis, *IEEE Electron Device Lett.*, 2006, **27**, 341–343.
27 Y. Civale, L. K. Nanver, P. Hadley, E. J. Goudena, H. W. van Zeijl and H. Schellevis, *Mater. Res. Soc. Symp. Proc.*, 2006, **940**, 0940-P05-04.